Instantaneous Degradation of Nerve Agent Simulants using Zirconium-based Metal-organic Polyhedra

Kimia Kiaei,[a] Andrzej Gładysiak,[a] Kieran Brunson,[a] Kye Hunter,[b] Ava Thomas,[a] Delaney Radke,[a] Tim Zuehlsdorff, [b] and Kyriakos C. Stylianou[a]*

[a]*Materials Discovery Laboratory (MaD Lab), Department of Chemistry, Oregon State University, Corvallis, OR, 97331-4003 USA*

[b]*Department of Chemistry, Oregon State University, Corvallis, OR, 97331-4003 USA*

Abstract: Metal-organic polyhedra (MOPs) are discrete molecules made of metal ions/clusters and organic ligands, and their crystal packing leads to the generation of intrinsic and extrinsic porosity. Due to their structural versatility, porosity, and nanoscale size, MOPs are considered an attractive platform for catalysis. In this study, we report for the first time the use of three zirconium(IV)-based MOPs for the degradation of trace concentrations of the nerve agent simulant, dimethyl 4-nitrophenyl phosphate (DMNP). All three MOPs degraded DMNP instantaneously, with half-lives ranging from $t_{1/2}$ = 17 to 130 s. The catalytic activity of MOPs is thought to be due to (1) their periodic packing resulting in long-range order that creates extrinsic porosity, allowing DMNP to diffuse in and interact with the pore surface and Lewis acids (Zr(IV) centers) of MOPs, and (2) the lability of Zr—Cp⁻ (Cp⁻ = cyclopentadienyl) bond, allowing Cp⁻ ligands to rearrange and make space for DMNP to interact with the Zr(IV). The catalytic activity of MOPs is not deteriorated by increasing the concentration of the nerve agent simulant nor in consecutive catalytic experiments, highlighting their robustness as catalysts. Our study showcases the promise of MOPs as one of the fastest active catalysts for the instantaneous degradation of nerve agents.

Keywords: metal-organic polyhedra, nerve agents, hydrolysis, extrinsic porosity, catalytic degradation

Fighting tactics changed during World War I when chemical warfare agents (CWA) were first deployed in 1914. The most prominent chemical weapon during WWI was mustard gas, 2,2'-dichlorodiethyl sulfide. This gas caused the formation of large blisters on exposed skin and in the lungs. Gas warfare agents during WWI accounted for 1-2% of deaths.[1] Later, more effective chemical killers were developed. It was found that organophosphate (OP) compounds were used as nerve agents (NAs) since they inhibited the acetylcholinesterase and caused muscle failure; this ultimately resulted in asphyxiation within minutes.[2] The terror surrounding chemical warfare agents (CWAs) resulted in a ban on OP NAs in 1997, where they received classification as agents of chemical terrorism.[3] The worldwide ban effectively prevented chemical weapons in large-scale warfare, but discrete instances of their use still exist.[4] These current uses of chemical warfare agents combined with modern-day stockpiles spur necessity in their decontamination, cleanup, degradation, and disposal.

Due to the severe toxicity of CWAs, less toxic OP compounds are used as analogs to study the degradation of CWAs. Methyl Paraoxon (dimethyl 4-nitrophenyl phosphate, DMNP) is a commonly used simulant for phosphate-based CWAs.[5] Like its toxic counterparts, DMNP can be hydrolyzed, forming non-hazardous products: dimethyl phosphate (DMP) and p-nitrophenoxide.[6] An active catalyst is required for the degradation and cleanup of DMNP. Many catalysts have been employed to study the degradation of DMNP, including inorganic bases, metal ions, and enzymes.[7] These catalysts have encountered several challenges, namely that homogenous catalysts are difficult or impractical to recycle. For this reason, research efforts shifted toward the development of heterogeneous catalysts.

Porous materials are promising candidates for DMNP degradation as they provide nano-confined spaces with unique chemical environments enhancing the rate of DMNP uptake followed by its hydrolysis. Among these materials are porous polymers,[8] metal-organic frameworks (MOFs),[9] and porous carbon in many forms, such as graphene,[10,11] nanotubes,[12,13] and activated carbon.[14,15] Porous polymers have shown promise, but their catalytic activity is limited to the type of nucleophile used as catalytically active material.[8] MOFs have shown great promise as heterogeneous catalysts in OP NA degradation.[16–18] MOFs are extended networks

made of metal ions or clusters and organic ligands.[19] They are catalytically active for DMNP hydrolysis since open Lewis acid sites can be generated through defects such as missing linkers in the crystal structure of the MOFs [20] or through coordinatively unsaturated metal sites.[21] The amino-functionalized UiO-66-NH$_2$ and UiO-67-NH$_2$, NU-1000, and MOF-808 are among the fastest-performing catalysts for the OP NA simulant degradation and have all been shown to catalyze DMNP hydrolysis with half-lives of less than 120 seconds.[16,22–27]

Similar to their framework counterparts, metal-organic polyhedra (MOPs) are another emerging class of materials that has only recently attracted attention as catalysts.[28–31] Like MOFs, MOPs are also composed of inorganic nodes and organic ligands. However, MOFs assemble into an extended framework composed of ordered pores. MOPs, on the other hand, are discrete nano-sized molecules. When MOPs pack into an extended lattice, these crystalline porous materials possess intrinsic (cavities within the metal-organic cages) and extrinsic (periodic channels or pores in the extended crystal lattice) porosity.[29,32–38]

Due to their structural similarities, MOPs and MOFs share important functional properties. Both materials are crystalline, porous, and tunable and possess metal centers that make them potentially effective catalysts.[33] In MOFs, introducing structural defects such as missing linkers (which result in exposing catalytically active metal sites) has been identified as a viable strategy to enhance the catalytic activity.[39,40] A similar role can be played by capping ligands in Zr(IV)-MOPs. Due to the Zr—Cp$^-$ (Cp$^-$: cyclopentadienyl) bond lability (i.e., thermodynamic instability of metal-carbon bonds compared to their hydrolysis product),[41] it is possible for Cp$^-$ capping ligands to rearrange and make space for guest or target molecules to interact with the metal ions, thus speeding up catalytic processes. In the event of Cp$^-$ ligand removal, for example, through hydrolysis and the cleavage of metal-carbon bonds, MOPs gain additional catalytic sites by further exposing the metal ions; the detachment of Cp$^-$ rings in metallocenes has been seen only after several hours in the solution.[41,42]

There are currently a few reports on MOPs for OP compound treatment.[37,43,44] Nitschke *et al.* synthesized a tetrahedral Fe-diaminoterphenylene based MOP that is

catalytically active in the hydrolysis of the NA simulant Dichlorvos. Quantitative degradation of Dichlorvos occurs in 96 hours when 1 mol% loading of MOP catalyst is used.[44] Similar degradation times were also shown by Ward *et al.* reporting that the degradation of a variety of OP compounds is thought to be occurring outside the cavity of the cage.[37] The studies listed above discussed homogeneous catalysis with the MOPs dissolved in the solution. Inspired by these studies, herein, we report the use of Zr-based MOPs as heterogeneous catalysts for the degradation of DMNP.

Three Zr-MOPs were prepared using zirconocene dichloride as the metal source and aromatic carboxylate ligands terephthalic acid (1,4-benzene dicarboxylic acid, BDC) and its amino-functionalized counterpart (BDC-NH$_2$) and trimesic acid (1,3,5-benzene tricarboxylic acid, BTC) (sections S1.2-4).[45,46] Structures of each Zr(IV) MOP tetrahedra are shown in Figures 1 and S1. Each MOP has four trinuclear Zr$_3$O(Cp)$_3$ metal-oxo clusters. These trinuclear Zr$_3$O clusters are linked either through four aromatic ligands centered on the faces of a tetrahedron (**Zr-BTC**) or by six aromatic ligands which form the edges of a tetrahedron (**Zr-BDC**, **Zr-BDC-NH$_2$**). Upon linkage of the four Zr$_3$O clusters through the aromatic ligands, a molecular cage is formed with an inner cavity with a diameter of 3.7 Å for **Zr-BDC** and 2.3 Å for **Zr-BTC**.[45] Formation of an extended lattice through crystallization of the molecular MOPs results in additional porosity extrinsic to the molecule. The extrinsic pore aperture can be estimated as canals with a diameter of ~6.1 Å (Figure 1).[45,47]

Successful syntheses of the MOPs were confirmed using powder X-ray diffraction (PXRD, Figures S2a-c), Fourier-transform infrared spectroscopy (FTIR, Figure S3), and thermogravimetric analysis (TGA, Figure S4). FTIR spectra confirmed the formation of MOP structures as they show no O—H bond stretching from carboxylic acid groups at the range of 3000 cm^{-1} (Figures S3a-c).[48] TGA analyses show similar thermal stability for all three MOPs where guest solvent molecules are removed by about 200 °C, and their degradation occurs at 300 °C.[45] The specific surface areas of the three MOPs were calculated using the Brauner-Emmet-Teller (BET) method from nitrogen isotherms (Figure S5). The BET surface areas for **Zr-BTC**, **Zr-BDC** and **Zr-BDC-NH$_2$** were found to be 365, 338, and 298 m^{2}g^{-1}, respectively.

Upon complete characterization of the three Zr-MOP materials, DMNP degradation studies were undertaken to assess their catalytic activity. The hydrolysis of DMNP was monitored by phosphorous nuclear magnetic resonance (NMR) spectroscopy with proton decoupling (^{31}P-{^{1}H}-NMR). The three crystalline Zr-MOPs were used to degrade methyl paraoxon at room temperature with *N*-ethyl morpholine buffer to regulate the pH above 8.5.[49] The catalyst (0.0006 mmol of each MOP) was mixed in the buffered solution with DMNP (0.001 mmol), and the reaction was allowed to proceed for a few minutes (section S1.6). Examining the mechanism of DMNP hydrolysis yields insights into the effects of porosity and structural integrity of MOPs. We found that all three Zr-MOPs can facilitate the hydrolysis of DMNP. The production of DMP (resulting from the breakdown of DMNP) occurs through the cleavage of the bond between phosphorous and the nitrophenyl group. The other DMNP degradation product, methyl 4-nitrophenyl phosphate (M4NP), results from the cleavage of the methyl C—O bond.[8,50] The peaks for M4NP have not been detected in the ^{31}P-NMR spectra of the degradation products for any of our MOP samples.

The DMNP degradation studies, along with the $Zr_3O(Cp)_3$ node structure and kinetics data, are presented in Figure 2. The three MOPs yielded fast catalytic hydrolysis of DMNP, with **Zr-BTC** being the faster catalyst to hydrolyze DMNP in less than 180 seconds, followed by **Zr-BDC** and **Zr-BDC-NH₂** MOPs. Control DMNP hydrolysis experiments with zirconocene dichloride (Figures S6-7, no MOP catalyst) showed 0% degradation after 5 minutes, confirming that these MOPs are catalytically active. The half-lives of the DMNP hydrolysis reactions were calculated based on the pseudo-first-order kinetics model as suggested by previous literature[51–53] by linear fitting of the natural log of the DMNP concentration vs. time and dividing the value of *Ln(2)*, or 0.6931, by the negative of the slope of the linear curves. Calculated half-lives were $t_{1/2}$ = 17, 80, and 129 s for **Zr-BTC**, **Zr-BDC**, and **Zr-BDC-NH₂**, respectively.

The short degradation half-lives of the Zr-MOP catalysts show that their performance is comparable to UiO-66-NH₂/polymer composites and other MOFs that have been tested previously.[26, 50] After the complete degradation of DMNP with **Zr-BTC** in the buffer solution, a second dose of 0.001 mol DMNP was added to the reactor, and a 100% degradation was observed for the second cycle. This suggests that the **Zr-BTC** MOP maintains its activity for DMNP degradation after a two-fold increase in DMNP

concentration (Figure S8). Comparing the fingerprint regions of the FT-IR spectra for the Zr-MOPs before and after DMNP degradation further supports the stability of the structure (Figure S9). The BET surface area for **Zr-BTC** MOP after two catalytic cycles was found to be 265 m^2/g, which is slightly lower compared to the fresh MOP, but a significant fraction of its BET was retained.

Comparing the catalytic activity of the three Zr-MOPs, the shortest DMNP hydrolysis half-life was observed with **Zr-BTC,** followed by **Zr-BDC** and **Zr-BDC-NH$_2$**. Their different catalytic activity (in terms of degradation half-life) is thought to be due to the difference in the Lewis acidity of Zr(IV) in each MOP. In **Zr-BTC**, each benzene ring is shared between three Zr(IV) centers, and in **Zr-BDC**, the benzene rings are shared between two Zr(IV) centers. The shared benzene rings in **Zr-BTC** make the Zr(IV) centers have a higher Lewis acidity than the Zr(IV) in **Zr-BDC**. Comparing the **Zr-BDC** and its amino-functionalized counterpart, electron-donating NH$_2$ functional groups in **Zr-BDC-NH$_2$** can have a similar effect by reducing the Lewis acidity of the Zr(IV) centers, resulting in the slightly slower DMNP degradation rate. This is contrary to the catalytic activity seen in amino-functionalized Zr-MOFs. Based on previous reports, the presence of amino-functional groups in UiO-66 has shown a remarkable reduction in the degradation half-life of DMNP.[22, 26] This is because amino functional groups cause changes in the microsolvation at the proximity of the accessible catalytic sites (i.e., missing linkers) in the MOFs resulting in faster catalysis. We suggest that despite structural similarities, the effects of amino groups are different in the tetrahedral Zr-MOPs compared to UiO-66 because of the crystal packing of MOPs and Zr(IV)—Cp$^-$ bond lability.

The aperture of the open face of a single Zr-MOP tetrahedron is ~3 Å,[45] making the intrinsic porosity of the molecule incapable of hosting DMNP (with a kinetic diameter of 4.5 Å);[54] however, the ~6 Å extrinsic apertures observed in the extended crystal lattice are sufficient to accommodate DMNP. Therefore, we hypothesize that DMNP hydrolysis occurs outside the cages in the voids between the tetrahedra – the extrinsic porosity (Figures 1b-d). Guest molecules, thus, play a vital role in maintaining the integrity of the extended lattice in MOPs. The removal of lattice *N,N*-diethyl formamide solvent molecules, through activation of MOPs, caused a crystalline to amorphous transition, resulting in the collapse of the extended and long-range order of the

MOPs.[29,45] When the activated **Zr-BTC** MOP (amorphous) was used for DMNP degradation experiments, it showed lower catalytic activity (63% degradation in 120 s) compared to its as-synthesized counterpart (97% degradation in 120 s) (Figure S10). The activated MOPs were subsequently set aside in favor of their better-performing pristine crystalline counterparts. This, in turn, suggests that the extrinsic porosity and crystallinity of the MOP crystal structures play an integral part in the catalytic process for DMNP hydrolysis. Another unique attribute of MOPs is the presence of capping Cp^- ligands in a 1-to-1 ratio with Zr(IV). The Cp^- ligands in an aqueous environment may detach from the Zr_3O clusters or be re-arranged through hydrolysis and provide Zr(IV) active sites for catalysis.[41] To further investigate this, we analyzed the buffered solution at which catalytic hydrolysis of DMNP proceeded using Atmospheric Pressure Gas Chromatography-Mass Spectrometry (APGC-MS); however, there was no sign of any significant peaks for Cp^- or other Cp^- byproducts (Figure S11). Our data suggests that there is no detachment of Cp^- from the Zr-MOP catalysts. This is further supported by previous literature reporting that hydrolysis of metal—Cp^- bonds is slow.[42,55] To better understand the binding of DMNP to the Zr-MOP catalysts, we conducted a computational study and calculated the binding energies for Cp^- and DMNP in the **Zr-BDC** MOP. Computational analysis showed that the affinity of Zr(IV) centers for Cp^- is higher (-244.327 kJ mol^{-1}) than that of DMNP (-55.661 kJ mol^{-1}) in the MOPs. Density functional theory (DFT) calculations revealed that DMNP most likely binds to the Zr(IV) centers through its non-methylated O atom from the phosphate group (section S1.7, and Figure S12). DFT calculations show that upon removal of the Cp group, leading to the generation of open Zr(IV) sites, the adsorption of DMNP to the Zr(IV) sites is energetically favorable with a binding energy of -56.985 kJ mol^{-1}. A metastable complex is also predicted to form even when Cp groups are not released from the MOP, due to the non-directional and labile bonding between the Cp^- and Zr(IV) centers. In this scenario the Zr(IV)—Cp^- bonds elongate and share the Lewis acidic Zr(IV) catalytic sites with DMNP (binding energy: 29.99 kJ mol^{-1}). The high binding energy of Cp^- and the presence of a metastable intermediate which does not release Cp^- into solution support the experimental observations that there is no free Cp^- and that the MOPs retain their structural integrity after multiple catalytic cycles.

Based on our observations, the DMNP degradation pathway with Zr(IV)-MOPs is proposed in Figure 3. In the Zr-MOPs, Zr(IV) is six-coordinated to five O atoms (two

from the carboxylate O atoms of the organic ligands, two OH⁻ and one O^{2-} bridges) and another bond with Cp⁻. Our experimental observations and computational study indicate that under basic aqueous solutions, Cp⁻ groups may rearrange and make space for DMNP to interact with the active Zr(IV) centers (steps I-II, Figure 3). The coordination of DMNP can be further stabilized with hydrogen bonding with the OH⁻ bridges in the Zr_3 node (step III, Figure 3).[56] In step IV, *p*-nitrophenoxide is detached from the P atom and forms a complex by coordinating with the methyl group. Step V shows the interactions between the Zr(IV) and phosphate ion and the production of *p*-nitrophenoxide. Finally, in step VI, both products – *p*-nitrophenoxide and phosphoric acid are separated from the catalyst, which is regenerated for a consecutive DMNP degradation.

In conclusion, the catalytic efficacy of three Zr-MOPs was evaluated toward the degradation of DMNP. Upon exposure of DMNP to each of our three MOP catalysts, 100% degradation of DMNP was observed in a few minutes, half-lives ranging from $t_{1/2}$ = 17 to 130 s. We attribute the rapid catalytic performance of the Zr-MOPs to their extrinsic porosity, long-range order, and Zr—Cp bond lability, allowing DMNP to diffuse in their pores, interact with Zr(IV) sites, and be degraded. Our research findings pave the way for continued exploration of functional MOPs as catalysts. Since these are molecular catalysts, particle-size reduction (nanoscale) strategies while retaining their structural integrity and activity can lead to their integration on surfaces to generate functional devices for large-area nerve agent decontamination.

References

[1]   G. J. Fitzgerald, *Am. J. Public Health* **2008**, *98*, 611.

[2]   S. W. Wiener, R. S. Hoffman, *J. Intensive Care Med.* **2004**, *19*, 22–37.

[3]   S. Chauhan, S. Chauhan, R. D'Cruz, S. Faruqi, K. K. Singh, S. Varma, M. Singh, V. Karthik, *Environ. Toxicol. Pharmacol.* **2008**, *26*, 113–122.

[4]   L. K. Sydnes, *Nature* **2020**, *583*, 28–29.

[5]   M. Agrawal, D. F. Sava Gallis, J. A. Greathouse, D. S. Sholl, *J. Phys. Chem. C* **2018**, *122*, 26061–26069.

[6]   S.-Y. Moon, E. Proussaloglou, G. W. Peterson, J. B. DeCoste, M. G. Hall, A. J. Howarth, J. T. Hupp, O. K. Farha, *Chem. - A Eur. J.* **2016**, *22*, 14864–14868.

[7]   A. Zammataro, R. Santonocito, A. Pappalardo, G. T. Sfrazzetto, *Catalysts* **2020**, *10*, 881.

[8]   D. Jung, P. Das, A. Atilgan, P. Li, J. T. Hupp, T. Islamoglu, J. A. Kalow, O. K. Farha, *Chem. Mater.* **2020**, *32*, 9299–9306.

[9]   M. R. DeStefano, T. Islamoglu, S. J. Garibay, J. T. Hupp, O. K. Farha, *Chem. Mater.* **2017**, *29*, 1357–1361.

[10]   N. Anđelić, Z. Car, M. Čanađija, *Math. Probl. Eng.* **2019**, *2019*, 1–23.

[11]   I. Sayago, D. Matatagui, M. J. Fernández, J. L. Fontecha, I. Jurewicz, R. Garriga, E. Muñoz, *Talanta* **2016**, *148*, 393–400.

[12]   M. C. Horrillo, J. Martí, D. Matatagui, J. P. Santos, I. Sayago, J. Gutiérrez, I. Martin-Fernandez, P. Ivanov, I. Grcia, C. Cané, *Sensors Actuators B Chem.* **2011**, *157*, 253–259.

[13]   M. A. K. Khan, K. Kerman, M. Petryk, H. B. Kraatz, *Anal. Chem.* **2008**, *80*, 2574–2582.

[14]   D. A. Giannakoudakis, M. Barczak, M. Florent, T. J. Bandosz, *Chem. Eng. J.* **2019**, *362*, 758–766.

[15]   R. Kaiser, A. Kulczyk, D. Rich, R. J. Willey, J. Minicucci, B. MacIver, *Ind. Eng. Chem. Res.* **2007**, *46*, 6126–6132.

[16]   K. Ma, M. C. Wasson, X. Wang, X. Zhang, K. B. Idrees, Z. Chen, Y. Wu, S. J. Lee, R. Cao, Y. Chen, L. Yang, F. A. Son, T. Islamoglu, G. W. Peterson, J. J. Mahle, O. K. Farha, *Chem Catal.* **2021**, *1*, 721–733.

[17]   Y. Liu, A. J. Howarth, N. A. Vermeulen, S. Y. Moon, J. T. Hupp, O. K. Farha, *Coord. Chem. Rev.* **2017**, *346*, 101–111.

[18]   Y. Liao, T. Sheridan, J. Liu, O. Farha, J. Hupp, *ACS Appl. Mater. Interfaces* **2021**, *13*, 30565–30575.

[19]   H. Furukawa, K. E. Cordova, M. O'Keeffe, O. M. Yaghi, *Science (80-.).* **2013**, *341*, 1230444.

[20]   O. V. Gutov, M. G. Hevia, E. C. Escudero-Adán, A. Shafir, *Inorg. Chem.* **2015**, *54*, 8396–8400.

[21]   Ü. Kökçam-Demir, A. Goldman, L. Esrafili, M. Gharib, A. Morsali, O. Weingart, C. Janiak, *Chem. Soc. Rev.* **2020**, *49*, 2751–2798.

[22]   M. J. Katz, S. Y. Moon, J. E. Mondloch, M. H. Beyzavi, C. J. Stephenson, J. T. Hupp, O. K. Farha, *Chem. Sci.* **2015**, *6*, 2286–2291.

[23]   H. Liang, A. Yao, X. Jiao, C. Li, D. Chen, *ACS Appl. Mater. Interfaces* **2018**, *10*, 20396–20403.

[24] M. C. De Koning, K. Ma, M. Van Grol, I. Iordanov, M. J. L. Kruijne, K. B. Idrees, H. Xie, T. Islamoglu, R. P. T. Bross, O. K. Farha, *Chem. Mater.* **2022**, *34*, 1269–1277.

[25] D. B. Dwyer, N. Dugan, N. Hoffman, D. J. Cooke, M. G. Hall, T. M. Tovar, W. E. Bernier, J. Decoste, N. L. Pomerantz, W. E. Jones, *ACS Appl. Mater. Interfaces* **2018**, *10*, 34585–34591.

[26] T. Islamoglu, M. A. Ortuño, E. Proussaloglou, A. J. Howarth, N. A. Vermeulen, A. Atilgan, A. M. Asiri, C. J. Cramer, O. K. Farha, *Angew. Chemie Int. Ed.* **2018**, *57*, 1949–1953.

[27] R. Gil-San-Millan, E. López-Maya, M. Hall, N. M. Padial, G. W. Peterson, J. B. DeCoste, L. M. Rodríguez-Albelo, J. E. Oltra, E. Barea, J. A. R. Navarro, *ACS Appl. Mater. Interfaces* **2017**, *9*, 23967–23973.

[28] H. Huang, Z. Y. Liu, S. B. Li, J. Zhu, B. X. Jiang, Y. T. Zhang, *J. Solid State Chem.* **2022**, *307*, 122821.

[29] A. J. Gosselin, C. A. Rowland, E. D. Bloch, *Chem. Rev.* **2020**, *120*, 8987–9014.

[30] A. C. Ghosh, A. Legrand, R. Rajapaksha, G. A. Craig, C. Sassoye, G. Balázs, D. Farrusseng, S. Furukawa, J. Canivet, F. M. Wisser, *J. Am. Chem. Soc.* **2022**, *144*, 3626–3636.

[31] W. H. Xing, H. Y. Li, X. Y. Dong, S. Q. Zang, *J. Mater. Chem. A* **2018**, *6*, 7724–7730.

[32] E.-S. M. El-Sayed, Y. Di Yuan, D. Zhao, D. Yuan, *Acc. Chem. Res.* **2022**, *55*, 1546–1560.

[33] B. S. Pilgrim, N. R. Champness, *Chempluschem* **2020**, *85*, 1842–1856.

[34] M. Sun, Q. Q. Wang, C. Qin, C. Y. Sun, X. L. Wang, Z. M. Su, *Chem. – A Eur. J.* **2019**, *25*, 2824–2830.

[35] D. J. Tranchemontagne, Z. Ni, M. O'Keeffe, O. M. Yaghi, *Angew. Chemie Int. Ed.* **2008**, *47*, 5136–5147.

[36] Z. Yang, N. Zhang, L. Lei, C. Yu, J. Ding, P. Li, J. Chen, M. Li, S. Ling, X. Zhuang, S. Zhang, *JACS Au* **2022**, *23*, jacsau.1c00556.

[37] C. G. P. Taylor, A. J. Metherell, S. P. Argent, F. M. Ashour, N. H. Williams, M. D. Ward, *Chem. - A Eur. J.* **2020**, *26*, 3065–3073.

[38] A. Carné-Sánchez, J. Albalad, T. Grancha, I. Imaz, J. Juanhuix, P. Larpent, S. Furukawa, D. Maspoch, *J. Am. Chem. Soc.* **2019**, *141*, 4094–4102.

[39] S. Dissegna, K. Epp, W. R. Heinz, G. Kieslich, R. A. Fischer, *Adv. Mater.* **2018**, *30*, 1704501.

[40] Z. Fang, B. Bueken, D. E. De Vos, R. A. Fischer, *Angew. Chemie Int. Ed.* **2015**, *54*, 7234–7254.

[41] A. Lubineau, J. Augé, M.-C. Scherrmann, *Aqueous-Phase Organomet. Catal.* **2005**, 25–43.

[42] M. K. Minacheva, E. M. Brainina, O. A. Mikhailova, Z. S. Klemenkova, B. V.

Lokshin, O. D. Rudyakova, G. I. Timofeeva, *Bull. Acad. Sci. USSR Div. Chem. Sci.* **1987**, *36*, 824–829.

[43] P. Delgado, J. D. Martin-Romera, C. Perona, R. Vismara, S. Galli, C. R. Maldonado, F. J. Carmona, N. M. Padial, J. A. R. Navarro, *ACS Appl. Mater. Interfaces* **2022**, *14*, 26501–26506.

[44] J. L. Bolliger, A. M. Belenguer, J. R. Nitschke, *Angew. Chemie Int. Ed.* **2013**, *52*, 7958–7962.

[45] G. Liu, Z. Ju, D. Yuan, M. Hong, *Inorg. Chem.* **2013**, *52*, 13815–13817.

[46] D. Nam, J. Huh, J. Lee, J. H. Kwak, H. Y. Jeong, K. Choi, W. Choe, *Chem. Sci.* **2017**, *8*, 7765–7771.

[47] G. Liu, Z. Yang, M. Zhou, Y. Wang, D. Yuan, D. Zhao, *Chem. Commun.* **2021**, *57*, 6276–6279.

[48] J. Workman, *Concise Handbook Of Analytical Spectroscopy, The: Theory, Applications, And Reference Materials: Volume 1: Ultravoilet Spectroscopy*, **2016**.

[49] S. Y. Moon, E. Proussaloglou, G. W. Peterson, J. B. DeCoste, M. G. Hall, A. J. Howarth, J. T. Hupp, O. K. Farha, *Chem. - A Eur. J.* **2016**, *22*, 14864–14868.

[50] K. Kiaei, M. T. Nord, N.-C. Chiu, K. C. Stylianou, *ACS Appl. Mater. Interfaces* **2022**, *14*, 19747–19755.

[51] S. Zboray, K. Efimenko, J. L. Jones, J. Genzer, *Ind. Eng. Chem. Res.* **2021**, *60*, 8799–8811.

[52] J. Zhao, D. T. Lee, R. W. Yaga, M. G. Hall, H. F. Barton, I. R. Woodward, C. J. Oldham, H. J. Walls, G. W. Peterson, G. N. Parsons, *Angew. Chemie* **2016**, *128*, 13418–13422.

[53] A. Yao, X. Jiao, D. Chen, C. Li, *ACS Appl. Mater. Interfaces* **2020**, *12*, 18437–18445.

[54] K. Vellingiri, L. Philip, K. H. Kim, *Coord. Chem. Rev.* **2017**, *353*, 159–179.

[55] J. H. Toney, T. J. Marks, *J. Am. Chem. Soc.* **1985**, *107*, 947–953.

[56] H. Chen, P. Liao, M. L. Mendonca, R. Q. Snurr, *J. Phys. Chem. C* **2018**, *122*, 12362–12368.

[57] M. C. De Koning, M. Van Grol, T. Breijaert, *Inorg. Chem.* **2017**, *56*, 11804–11809.
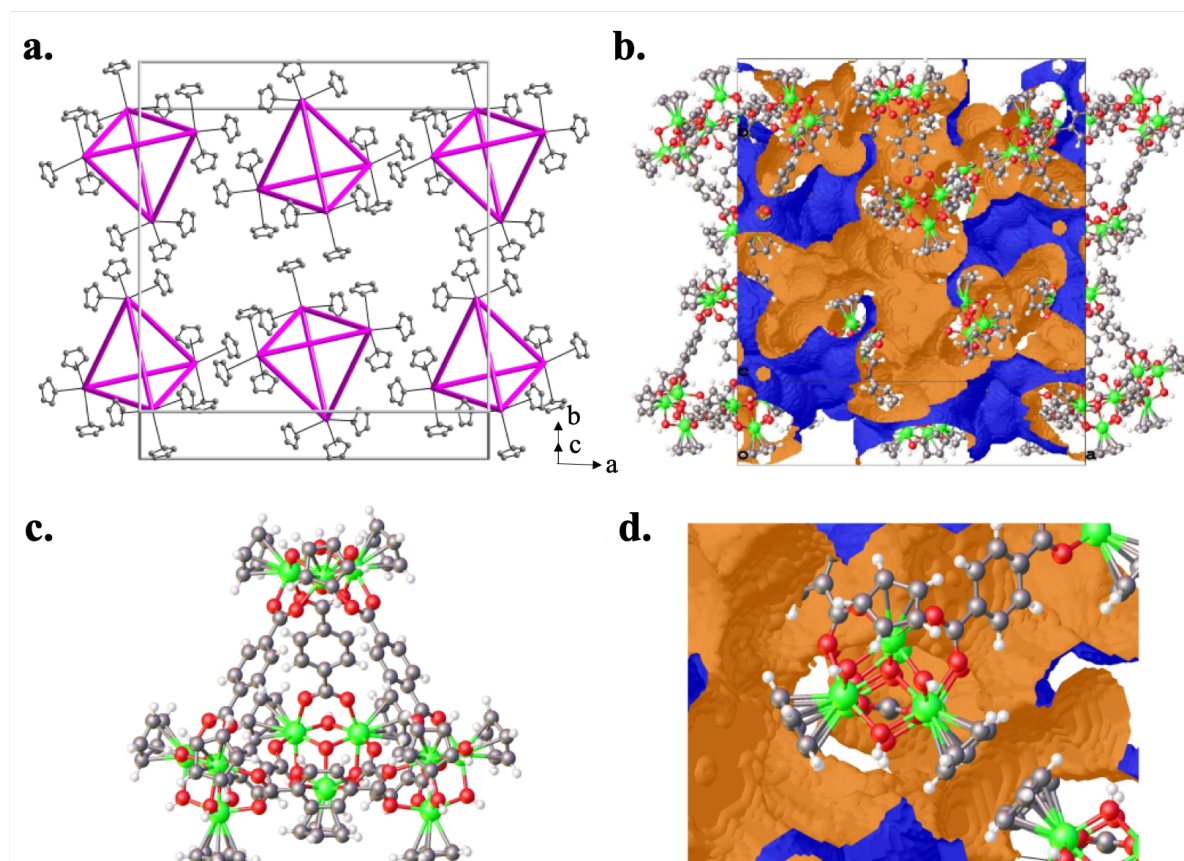
Figures and Tables.

Figure 1. (a) Arrangement of **Zr-BDC** MOP within its tetragonal unit cell. Gray spheres represent C atoms of the Cp⁻ ligands, while pink rods represent the Zr_3O-interconnected BDC ligands. (b) A system of structural voids within the crystal structure of **Zr-BDC** that accounts for 48.9% of its unit-cell volume. The outer surface of the structural void is marked in orange, while the inner surface in blue. Both views are toward the $(0\bar{1}2)$ plane. (c) An individual **Zr-BDC** MOP. (d) A detail of the crystal structure of **Zr-BDC** MOP featuring the environment of the Zr_3O cluster. Cp⁻ ligands are lined with the outer surfaces of the structural voids. Color code: C, gray; H, white; O, red; Zr, light green.
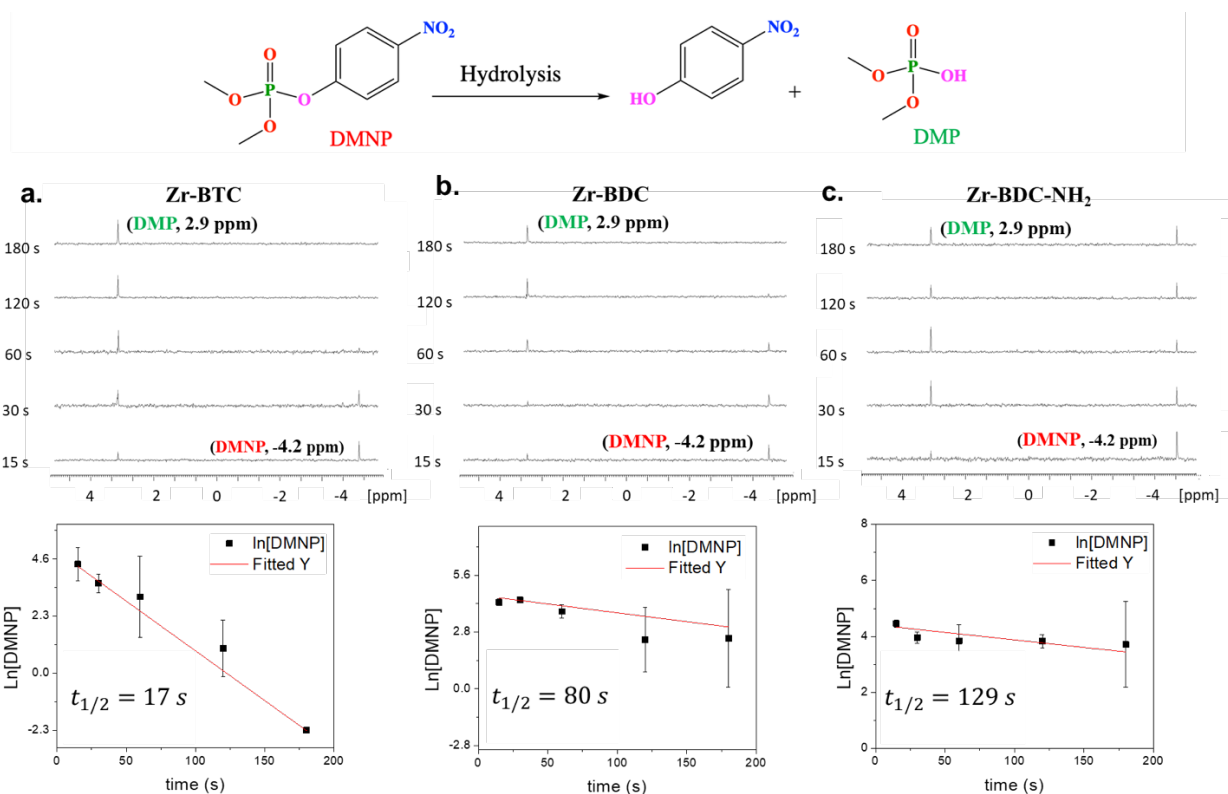
Figure 2. The hydrolysis of DMNP produces *p*-nitrophenoxide and dimethyl phosphate (DMP). The ^{31}P-NMR spectra of buffered DMNP solution show degradation times of 15 to 120 s for **a. Zr-BDC**, **b. Zr-BDC-NH$_2$** and **c. Zr-BTC** MOPs as catalysts followed by the pseudo-first-order model fitting of DMNP degradation with their calculated half-lives, $t_{1/2}$. The $t_{1/2}$ of for **a. Zr-BTC**, **b. Zr-BDC**, and **c. Zr-BDC-NH$_2$** are 17, 80, and 129 s, respectively.
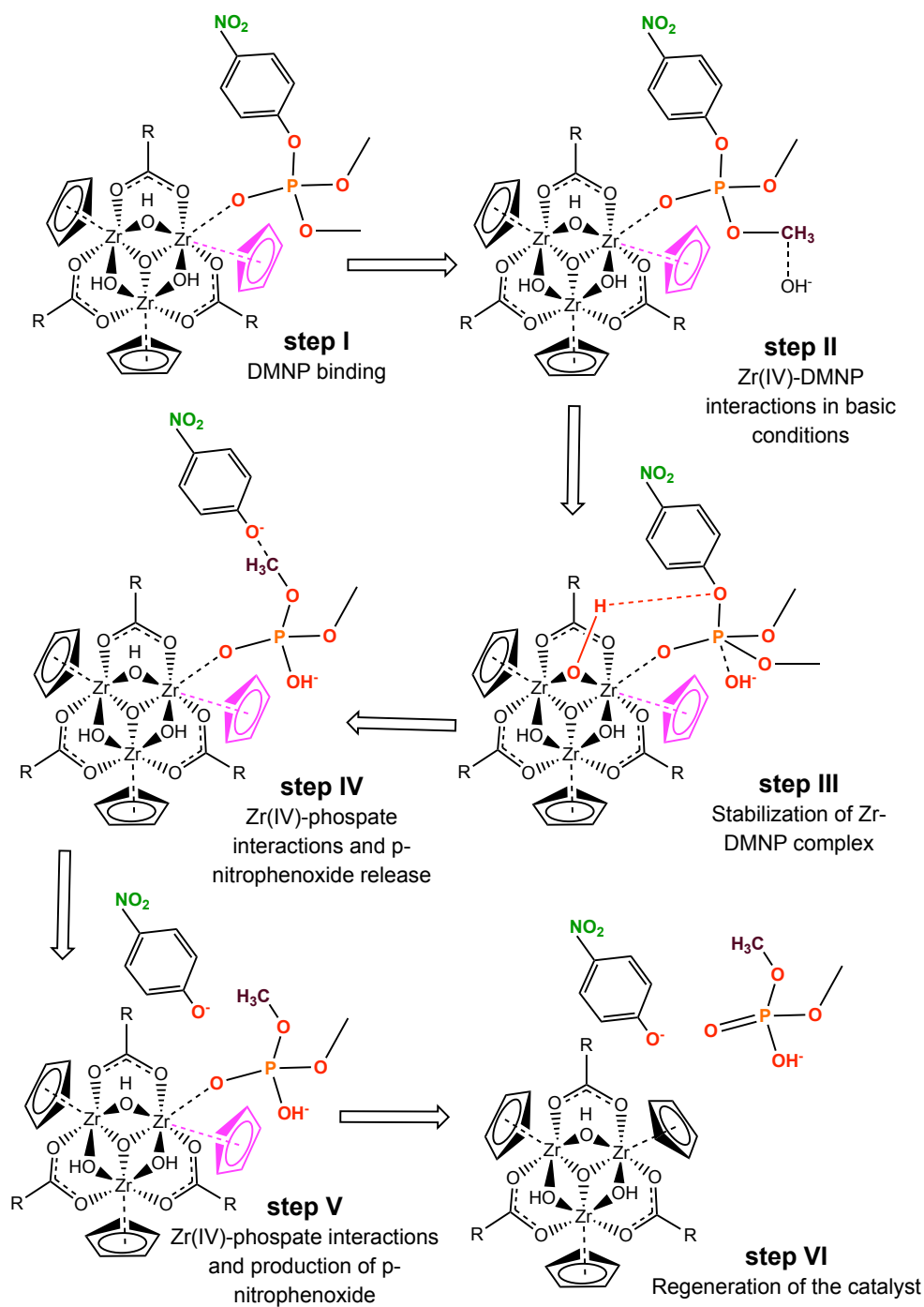
14

Figure 3. Proposed pathway for DMNP degradation with the Zr_3 nodes in the tetrahedral Zr-MOPs.